IEEE Robotics and Automation Letters (RA-L) paper, presented at ICRA 2026, Vienna, Austria. Cite as RA-L paper.

The Folding Hand: Anthropomorphic Robotic Hands with a Compact Reconfigurable Humanoid Palm Design

Qiujie Lu*[1], Jiehan Zou*[1], Zhongxue Gan[1]

***Abstract*— The human palm is a remarkable and highly functional part of the hand that significantly contributes to dexterity, grasp versatility, and overall manipulation capability. The metacarpophalangeal joints (MCP) of the palm facilitate movement of the fingers for flexion, extension, abduction, adduction, and limited circumduction, which can be a challenge to replicate the same function in robotic hands by simple design. In this paper, we proposed a single actuated folding mechanism as the metacarpals and passive rotating MCP joints to perform abduction, adduction, and circumduction of the human hand. The proposed anthropomorphic hand called Folding Hand which has a reconfigurable palm and five underactuated tendon-driven fingers. The design of the hand is compact and the price is low, with all six actuators and five sensors on the hand costing less than $180. Additionally, a methodology has been developed to comprehensively analyze the grasping capacity by combining the grasping quality and the grasping workspace. The experimental results show that the folding palm mechanism and the compliant rotating finger base can replicate human hand capabilities and performance precision and in-hand manipulation tasks.**

I. Introduction

Fully actuated high-DOF anthropomorphic robotic hands offer significant advantages in tasks that require dexterity, precision, and versatility, allowing robots to manipulate objects similarly to humans [1]–[3]. However, these robotic hands are typically more complex and expensive to develop and maintain compared to simpler robotic hands. Their advanced mechanics and sensors require significant energy and computational power [4], [5]. Furthermore, achieving the same level of dexterity and adaptability as human hands remains a challenge, and the reliance of the robot on intricate hardware can make it vulnerable to mechanical failure and the complexity of control algorithms and the need for real-time adaptability also pose significant challenges [6].

Simplified underactuated anthropomorphic robotic hands are designed with fewer actuators and sensors, allowing them to achieve complex and adaptive movements with less hardware [7]. By utilizing passive mechanical elements such as springs and tendons, these hands can passively adapt to the shape and size of objects they grasp, providing a more efficient and lightweight design compared to fully actuated hands [8]. While they can perform a wide range of grasping tasks, their reduced number of actuators limits their precision and control, making them less suitable for tasks that require fine manipulation or high levels of dexterity [9].

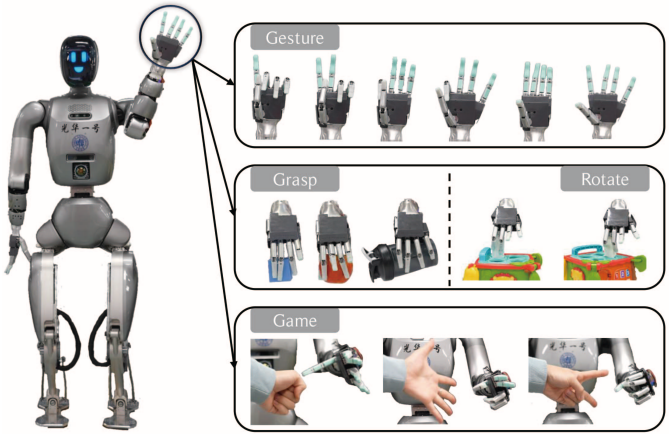

Fig. 1: The Folding Hand on GuangHua I humanoid robot, **Top**: abduction and adduction performance of the folding palm mechanism which helps the hand to demonstrate more anthropomorphic gestures. **Middle**: versatile adaptive grasping and in-hand manipulation with the compliant rotating finger base and the folding palm mechanism. **Bottom**: interactive activities, e.g. the paper-scissors-rock.

The human palm plays an essential role during grasping and manipulation tasks, the same as the robotic hand [10]. A growing body of work has focused on improving the functionality of the palm of robotic hands to enable versatile and robust manipulation. Capsi-Morales et al. [11] investigated palm concavity and adaptability of Pisa/IIT SoftHand, highlighting its critical role in enhancing the stability and adaptability of the grasp in real-world tasks. The BarrettHand [12] allows two fingers to rotate around the central palm axis via gear-based actuation, enabling multiple grasp configurations. Gao et al. [13] modified the BarrettHand into a five-finger anthropomorphic hand capable of shifting finger configurations to perform different grasping tasks. The MetaHand [14] and its variants [15] explore kinematic reconfigurability through palm designs based on spherical or planar linkage. Similarly, Lu et al. [16] presented a three-actuator design, where two actuators reconfigure the palm and one drives all underactuated fingers. However, palm movements in these designs do not conform to the biological characteristics of the human hand.

In this paper, we present a simplified anthropomorphic robotic hand featuring a compact, low-cost (approximately $180), and highly functional design. The hand achieves palm reconfigurability using only a single servo motor to coordinate the adduction and abduction of all finger bases in a coupled

*Q. Lu and J. Zou contributed equally to this paper.

This work was supported by the Natural Science Foundation of China under Grant 52305013, the Shanghai Pujiang Program under Grant 22PJD006, and the Shanghai Municipal Science and Technology Major Project (No.2021SHZDZX0103), Shanghai Engineering Research Center of AI & Robotics, Fudan University, China., Engineering Research Center of AI & Robotics, Ministry of Education, China.

[1]College of Intelligent Robotics and Advanced Manufacturing, Fudan University, 200433, Shanghai, China. (e-mail: {qj_lu, ganzhongxue}@fudan.edu.cn)

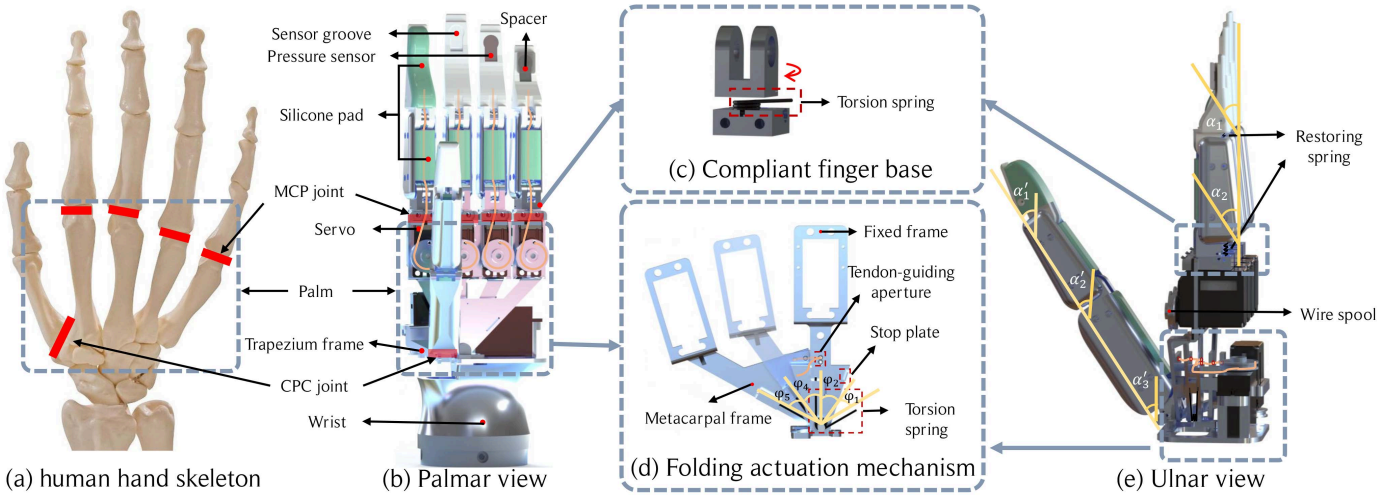

Fig. 2: (a) Diagram of the human hand skeleton. (b) Palmar view: Hand in the adduction state, showing essential structural components and finger tendon routing. (c) Structural illustration of the compliant finger base. (d) Structural design of the tendon-driven folding mechanism. (e) Ulnar view: Additional structural components and tendon routing for palm folding actuation.

manner, mimicking the motion of the human palm. This is implemented via a tendon-driven mechanism that enables both active reconfiguration and passive adaptability during grasping. Additionally, a self-adaptive rotating base at each finger-root mimics the MCP joints of the human hand to provide compliant in-hand rotation and improved object enclosure. Unlike previous designs with high actuation redundancy, our approach emphasizes mechanical simplicity and synergy, enabling stable anthropomorphic grasping and object-invariant in-hand manipulation using only six actuators. Furthermore, we propose an object-independent grasp workspace generation method and a grasp capability evaluation approach to comprehensively assess grasping performance under different hand configurations.

II. The Folding Hand

A. Design of the Fingers

Fig. 2b illustrates the appearance and structural features of the Folding Hand, which comprises five fingers, each independently tendon driven by a servo motor. Each fingertip is equipped with a pressure sensor and covered with a layer of silicone skin that extends along the phalanges, enhancing contact friction and ensuring secure grasping. A designed spacer is embedded between the sensor and the silicone layer to concentrate external force onto the pressure sensor. Fig. 2c highlights the compliant rotating finger base. Each finger is mounted on a torsional spring that enables passive adaptation to object geometry during grasping and manipulation.

B. Design of the Palm

To emulate the abduction and adduction of human metacarpophalangeal joints, we designed a simple yet effective fan-shaped mechanism, actuated by a single servo motor, as shown in Fig. 2d. The metacarpal frames are arranged symmetrically along the middle finger and are interconnected via torsional springs. These springs provide the restoring force required for palm abduction. In addition, mechanical stop plates are incorporated to restrict the compression and abduction range of the frame. Two tendons are routed through the guide holes in the frames, originating from the little finger and the thumb, converging to the middle finger, and terminating on the servo pulley. The servo provides the adduction motion of the palm. All five fingers are connected to the metacarpal frames to form a conventional anthropomorphic robotic hand architecture, resulting in a total of six degrees of actuation (DoA): five DoAs correspond to the flexion/extension of the individual fingers, and the sixth DoA is dedicated to palm abduction.

C. Prototype Parameters

The folding hand was designed to be easily 3D printed by resin, which allowed fast and cheap prototyping. In this paper, for better robustness of the performance, the folding hand was machined with aluminum alloy 3060. Five flexiforce A101 sensors were attached to each fingertip covered with Smooth-Sil 960 silicone outer layer. The sensors were calibrated by Handpi tensile testing machine. The torsional spring for the adaptive fingerbase is 0.4*5*3*60 (wire diameter*outer diameter*total coils*free position) and for the folding palm is 0.7*4*3*60. The stiffness of the spring is chosen by the weight of the finger structure. Five fingers were actuated by HPS-0618SG servo motors, and the palm was actuated by a KST A13-610 servo motor. The dimensions of the hand are 203 × 72 × 45 mm, with a weight of 440 g. The maximum flexion angles of the thumb joints α'_{1-3} are 116°, 111°, and 106°. Similarly, the maximum flexion angles of other fingers joints $\alpha_{1,2}$ are 116° and 104°, symbols indicated in Fig. 2e . The metacarpal frames of the thumb, index finger, ring finger, and little finger can abduct laterally from the middle finger φ by 39°, 37°, 46°, and 46° respectively. Additionally, the compliant finger base rotating range is ±18°. All servo motors and force sensors were connected to STM32F103C8T6 board, and attached to the humanoid robot Guanghua I.

III. Modelling of Folding Hand Operation Workspace

A. Kinematic Analysis of the Folding Hand

The reachable workspace of a robotic hand is defined as the set of points that can be attained across all feasible motion configurations. It quantitatively characterizes the spatial extent within which the hand can perform tasks. Due to the reconfigurability of the relative position of the palm, variations in palm morphology must be considered when analyzing finger kinematics.

As shown in Fig. 3a, the set of fingers is defined as $S = \{1, 2, 3, 4, 5\}$, where 1 to 5 represent thumb, index, middle, ring, and little fingers, respectively. The folding hand kinematic model can be modelled as 5 serial kinematic chains located on a cylindrical joint b_h, defined as the base of the palm. The reachable workspace of the hand is computed as the union of the reachable sets of all five serial chains, subject to individual joint constraints and palm configuration parameters. The pose of a point k on finger $i \in S$, relative to the b_h, is given by:

$$T_{i,k} = {}^{b_h}_{b_{f_i}}T \cdot {}^{k}_{b_{f_i}}T, T_{i,k} \in SE(3) \tag{1}$$

where b_{f_i} is the local base frame of finger i.

Since finger bases incorporate adaptive rotating joints, their angular positions theoretically span the entire operating angle during task execution. When employing the Monte Carlo method to compute the reachable workspace, these adaptive joints are treated as active degrees of freedom. The palm is initially set to the adduction position and three scenarios are compared: fixed palm, compliant finger base, and folding palm with compliant finger base. The resulting reachable workspaces, illustrated in Fig. 3b-d, demonstrate that compliant finger base joints significantly expand the hand's operational range, while the folding palm further enhances workspace coverage. However, these analyses neglect force interactions; the grasping workspace analysis with the grasping constraints and force closure has been developed below.

Assume that the grasp configuration is $\Omega \subseteq S$, which must include the thumb. During the grasping of the object, the force at the contact point is assumed to cause hard contact with the surface (positive constraint), while the adhesive forces are disregarded. Here, we incorporated an analysis of all phalangeal contacts to investigate the performance of dexterous hands in a more general object grasping scenario.

Each finger $i \in \Omega$ has n_i joints, and the object's center of mass is at O_o indicated in Fig. 3a. Assume all parts of the object can achieve normal contact with the joints, resulting in no tangential friction. Possible contact points on the n_i-th joint are $o_{i,n} \in R^3$, and the relative position of the contact point to the center of object is $R_{i,n} = o_{i,n} - O_o \in R^3$. The moment exerted by the force on the joint is $M_{i,n} = R_{i,n} \times F_{i,n} \in R^3$. $C_i = [c_{i,1}, c_{i,2}, \cdots, c_{i,n_i}]^T \in R^{n_i}$ represents the contact state matrix of finger i, where $c_{i,n} = 0$ or 1 indicates whether is in contact (1 for contact). The total moment of all joints on finger i is $M_i = [M_{i,1}, \cdots, M_{i,n_i}]C_i \in R^3$. The force applied by finger i on the object is represented by the wrench

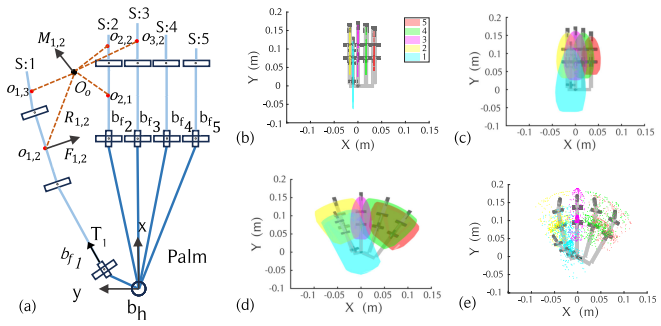

Fig. 3: (a) Kinematic model of the hand and schematic of object-independent grasping. (b)-(d) feasible workspaces for three hand states:fixed palm, compliant finger base, and folding palm with compliant finger base, respectively. (e) grasping workspace of the fingers under the folding palm with compliant bases.

$\omega_i = [F_i, M_i]^T$. The primary factor for successful grasping is the balance of wrenches, given by: $\omega_\Omega = \sum_{i \in \Omega} \omega_i = 0$.

Due to the shape of the object is unknown, we assume that the centroid O_o is located at the geometric center of all contact points. We define the space of all possible hand postures under different hand configurations that can achieve a grasp:

$$\mathcal{P} = \bigcup_{i \in \Omega} \{P_{i,n} \mid c_{i,n} = 1, n = 1, 2, \ldots, n_i\} \tag{2}$$

To compute the finger contact matrix of the Folding Hand, we analyze the driving forces acting on individual phalanges under nominal actuation. As shown in Fig. 4a and 4b, a tension spring is attached between the protrusions O_{3n_i+2n-3} and O_{3n_i+2n-2} on adjacent phalanges, with spring behavior transitioning through three states (P_1, P_2, P_3) as the phalanx rotates. The spring length $l_{n,s}$ varies with the rotation angle γ, and is defined as:

$$l_{n,s} = \begin{cases} \sqrt{l_{n-1}^2 + l_n^2 - 2l_{n-1}l_n \cos(A)}, & \gamma \le \gamma_c \\ \sqrt{l_{n-1}^2 - r_1^2} + \sqrt{l_n^2 - r_1^2} + Br_1, & \gamma > \gamma_c \end{cases} \tag{3}$$

where $l_{n,s}$ denotes the length of the tension spring. The angle A is defined as $\alpha_0 + \gamma$, while angle B is given by $\alpha_0 + \gamma - \gamma_c$. Here, γ represents the rotation angle of the n-th phalanx. The force of the tension spring can be expressed as $T_n = k_n(l_n - l_{n,s_0})$, where l_{n,s_0} represents the original length of the tension spring.

The force on the finger at the n-th phalanx in the direction perpendicular to the phalanx is:

$$F_{i,n} = \begin{cases} T(\cos\theta_{2n-1} - \cos\theta_{2n+1}) + \\ T_n \cos\theta_{2n_i+n-1} - T_{n+1}\cos\theta_{2n_i+n}, & n < n_i \\ T\cos\theta_{2n-1} + T_n \cos\theta_{2n_i+n-1}, & n = n_i \end{cases} \tag{4}$$

To exhibit the grasping workspace, considering the passive degrees of freedom in the finger as active degrees, with the torque given by $\tau_i = k_i\alpha_i$, where k_i is the torsional spring stiffness coefficient, and α_i is angle of the torsion spring. If the finger has only one contact point with the object, the spring generates torque producing a tangential force at the contact point. For multiple contact points, as the driver force forms only positive pressure, the torque at the finger base spring equals the friction torque at each contact point. Since static friction is proportional to joint force, the spring torque distribution at each contact point follows the joint

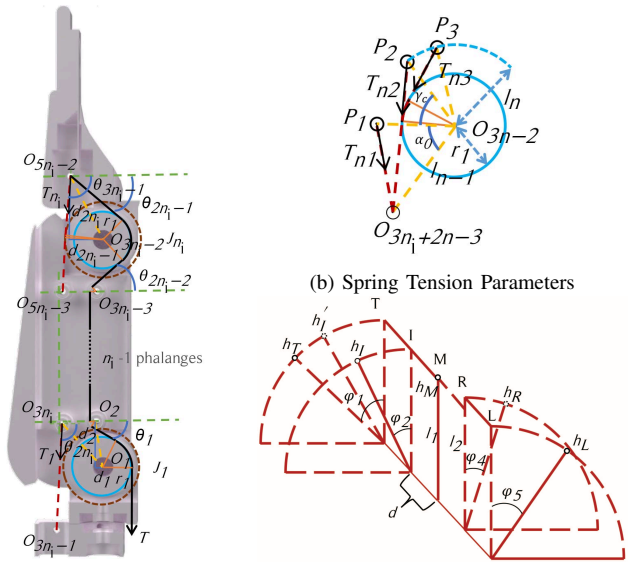

(a) Finger Parameters (b) Spring Tension Parameters (c) Palm Parameters

Fig. 4: Finger and palm parameters used for force constraint calculation in the grasping workspace. (a) Generalized parameters of the proposed tendon-driven fingers. J denotes the joints, and n_i is the number of joints in finger i. Blue solid rings represent the grooved bearings with outer radius r_1. The red dashed line indicates the dorsal tension spring, which connects to anchor points on both sides of the joint J. Black lines represent tendons. (b) Idealized spring tension variation between the nth and $(n-1)$th phalanges. The spring connects fixed points O_{3n_i+2n-3} and O_{3n_i+2n-2}, illustrating the geometric relationship during rotation and the transition through tension states at P_1 (initial position of O_{3n_i+2n-3}, finger not actuated), P_2 (contact point when the spring just touches the grooved bearing during rotation), and P_3 (position of O_{3n_i+2n-3} after continued rotation). (c) Folding palm parameters related to palm reconfiguration and workspace computation. h_T to h_L denote the tendon holes corresponding to the thumb through little finger metacarpal frames. ϕ_1 to ϕ_5 indicate the abduction angles of each metacarpal frame around the base axis. d represents the designed offset distance between anterior and posterior metacarpals.

force moment proportion. With the same friction coefficient, the total torque on the object exerted by finger i is $\tau_i = M_i + \sum_{n=1}^{n=n_i} \langle \lambda_{i,n} T_i, M_{i,n} \rangle$,$\lambda_{i,n} = \frac{\|F_{i,n} \times R_{i,n}\|}{\sum_{j=1}^{j=n_i} \|F_{i,j} \times R_{i,j}\|}$, where $\lambda_{i,n}$ indicates the distribution ratio of spring torque on the n-th joint, and $\langle \lambda_{i,n} T_i, M_{i,n} \rangle$ represents the torque allocated to the joint in the direction of the torque at the joint contact point. As shown in Fig. 3e, the grasping workspace of the five-fingered configuration—incorporating both a folding palm and a compliant finger base—is generated using the proposed method. This workspace serves as the foundation for our subsequent evaluation of graspability.

B. Comprehensive Grasp Capability Evaluation Based on Hand Configuration

This section presents a comprehensive, object-independent grasping capability evaluation method applicable to general robotic hands. It is based on an object-independent grasp workspace generation approach, which does not require strict constraints on predefined objects. Furthermore, coverage-based indicators and grasp quality metrics derived from the grasp matrix are examined to comprehensively evaluate grasping capability across different hand configurations.

We introduce the effective grasp coverage η, which quantifies the spatial capability of the hand. It is defined as the ratio between the volume of the graspable workspace $V_{\mathcal{P}}$ and the volume of the reachable workspace V_r:

$$\eta = \frac{V_{\mathcal{P}}}{V_r}. \tag{5}$$

To evaluate the grasp quality, the grasp matrix G has been conducted [17]:

$$G = \sum_{i \in \Omega} \left\{ \begin{bmatrix} I \\ \hat{R}_{i,n} \end{bmatrix} \Big|_{c_{i,n}=1,\, n=1,2,\ldots,n_i} \right\}, G \in R^{6\times 3N} \tag{6}$$

where N is the total number of contact points between the hand and the object $N = \sum_{i\in\Omega} \|C_i\|$, the contact force matrix $\tilde{F} \in R^{3\times N}$ and the resulting wrench matrix $\tilde{\omega} \in R^{3\times N}$ are related through the grasp matrix G, I is the 3×3 identity matrix and $\hat{R}_{i,n} \in R^{3\times 3}$ denotes the antisymmetric matrix corresponding to the moment arm from the object center to the n-th phalanx of finger i. It is computed as $\hat{R}_{i,n} = \tilde{\tau}_{i,n} \tilde{F}^{+}_{i,n}$, where $\tilde{\tau}_{i,n}$ is the torque and $\tilde{F}^{+}_{i,n}$ is the pseudoinverse of the contact force at that point.

To evaluate grasp quality under a given grasp configuration ω, we define two metrics:

$$MSSV(G) = \frac{1}{N} \sum_{n=1}^{N} SSV(G_n), \tag{7}$$

$$MVM(G) = \frac{1}{N} \sum_{n=1}^{N} VM(G_n), \tag{8}$$

where $SSV(G_n)$ and $VM(G_n)$ denote the smallest singular value and volume measure of the n-th grasp instance, respectively. $MSSV$ and MVM represent the mean SSV and VM under configuration Ω.

For uncertain grasps, a higher value of η indicates more extensive coverage of the hand's workspace, reflecting the hand's ability to effectively utilize its reachable space. MSSV and MVM quantify the lower bound and overall grasp stability of a given configuration, respectively, with higher values corresponding to increased grasp robustness. The volume used to compute η is determined using the Quickhull algorithm. These metrics collectively represent the grasping capability of a given hand configuration.

Considering only the contacts between the object and the fingers does not fully capture all grasping scenarios, as the palm may also contribute to object stabilization by applying additional forces to counteract torques and net forces. In such cases, it is assumed that the resultant force on the object is directed toward the palm, which provides adequate support, while friction between the palm and the object compensates for any residual torque. To evaluate the influence of palm configuration, we employ a weighted sum of composite indicators to select four representative grasp configurations that exhibit significant variation in palm structure—namely,

TABLE I: Metrics of five hand configurations with (F) and without (U) folding features.

Grasp Configuration Ω		MSSV	MVM	η
(1,2,3,4,5)	U	0.0597	0.0144	0.3706
	F	0.0773	0.0268	0.7412
(1,2,3,4)	U	0.0501	0.0072	0.3447
	F	0.0631	0.0119	0.8154
(1,2,4)	U	0.0403	0.0030	0.3187
	F	0.0488	0.0048	0.7783
(1,2,3)	U	0.0343	0.0022	0.2817
	F	0.0407	0.0027	0.4818
(1,5)	U	0.0249	0.0008	0.2928
	F	0.0245	0.0015	0.5559

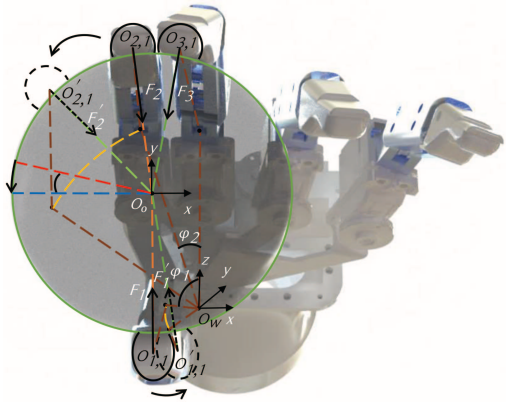

Fig. 5: Analysis parameters of the in-hand manipulation system.

with folding features (F) and without (U)—based on different numbers of involved fingers. Table I summarizes the grasping capability indicators for these four configurations and the grasp configurations used in the subsequent manipulation stage $\Omega = \{1, 2, 3\}$. The results suggest that, in theory, the inclusion of more fingers in the grasp configuration enhances robustness and improves workspace coverage, which is further strengthened by our palm folding design.

C. Dynamic Analysis of the Adaptive In-hand Manipulation

Two fingers can ordinarily achieve rotation around the x-axis. Rotation around the z-axis, in cases where the palm is not reconfigurable, typically requires the cooperation of the palm or more than four fingers [18]–[20]. The active degrees of freedom in the palm and the independent degree of freedom of the thumb allow us to achieve rotation around the z-axis with just three fingers, based on pressure-sensing sensors, thereby enabling more precise operations.

In-hand manipulation introduces multidirectional disturbances that affect the overall stability of the object. During the quasistatic process, it can be considered a sequence of stable grasping actions. Three-finger stability surpasses two-finger stability, and compared to four-finger configurations, three-finger configurations require fewer setups and consume less energy. Therefore, we consider using a three-finger configuration for in-hand manipulation. Among the three-finger configurations, the combination of the middle finger, index finger, and thumb ($\Omega = \{1, 2, 3\}$) exhibits the smallest variation in grasp quality evaluation performance, MVM, during the folding process, with a change value of 0.0005, as shown in Table I. This indicates that after grasping the object, the dynamic change in the palm has minimal impact on overall stability. Hence, this configuration can be selected to perform in-hand rotation tasks.

The analysis of in-hand rotation manipulation is shown in Fig 5. The initial positions of the thumb, index finger, and middle finger are at $O_{1,1}, O_{2,1}, O_{3,1}$, which can grasp a object. The base of the palm is defined as the global coordinate system O_w. Currently, the center of the object O_o are known. The angle between the index finger-palm connection and the middle finger-palm connection is φ_2, while the angle with the thumb-palm connection is φ_1. As shown in Fig. 4c, the length of the wire passing through the hand's aperture (on the thumb side) is calculated as:

$$L(\varphi_2, \varphi_1) = \sqrt{d^2 + l_1^2 \sin^2 \varphi_1 + l_1^2 (\cos \varphi_2 - \cos \varphi_1)^2} + \sqrt{d^2 + l_1^2 \sin^2 \varphi_2 + l_1^2 (1 - \cos \varphi_2)^2} + 2b \tag{9}$$

where d is the distance between the finger-palm connection plates, b is the thickness of the connection plate, and l_1 is the distance from the thumb-side connection plate to the palm base.

By controlling the actuation of the palm and fingertips, the thumb and index finger rotate around the object center O_o to new positions $O'_{1,1}$ and $O'_{2,1}$, respectively, utilizing static friction at the contact interfaces to achieve in-hand object rotation. A local coordinate system is established at the object center O_o. For the thumb and index finger, once the angles φ_1 and φ_2 are specified, the corresponding contact points on the object surface are uniquely determined according to 1 as

$$O^o_{i,1} = T^o_w T_{i,k} \quad \text{s.t.} \quad \|O^o_{i,1}\| = r \tag{10}$$

Where $O^o_{i,1}$ is the position of the fingertip of finger i in the object's coordinate system, and T^o_w is the homogeneous transformation from the global coordinate system to the object coordinate system.

When the position of the fingertip in the object's coordinate system is known, equations can be solved to determine the changes in tension required by the actuator. The fingertip sensor measures the contact force with the rotating object, with the effects of the torsion spring torque at the base of the fingers already included in the measured endpoint force, allowing for the analysis of the object's rotational state:

$$\begin{bmatrix} \widetilde{F} \\ \widetilde{\tau} \end{bmatrix} = \begin{bmatrix} 0 \\ J\alpha \end{bmatrix} \tag{11}$$

Here, $\widetilde{F}$ represents the force sensed by the fingertip acting on the object, distinguishing it from the joint driving force F produced during normal actuator operation in the previous section. J denotes the rotational inertia of the object, and the combined torque of the three fingers is $\widetilde{\tau} = \left[\widetilde{M}_1, \widetilde{M}_2, \widetilde{M}_3\right]^T$.

In the initial state of the system, the fingertips of all three fingers are in normal contact with the object. The middle and index fingers maintain no relative sliding with the object. The torsional springs on the finger bases adaptively rotate to keep the fingertips in normal contact with the object, the torsion angle determined by the position of the fingertip. For

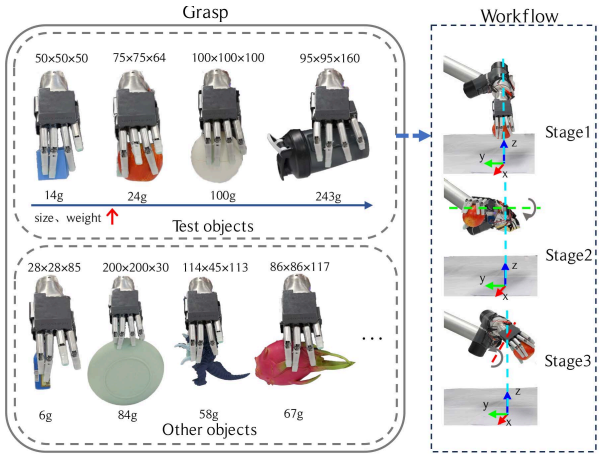

Fig. 6: **Left**: various grasping configurations on versatile objects with the dimensions(length×width×height, in mm on the top and weights at the bottom. **Right**: the testing process of the grasping experiments.

the torsion spring at the base of the finger T_i, the torque corresponds to the component of the fingertip torque at the root of the finger. Specifically, the position of the fingertip determines the required rotation angle of the torsion spring, which in turn dictates the force to be applied to the index and middle fingers. We discretize the rotational process over the entire period T into N steps, such that at the n-th time step t_n, the rotational angle of the object is given by:

$$\theta_{t_n} = \sum_{n=0}^{n=N} \alpha_{t_n} \frac{T}{N} \tag{12}$$

where α_{t_n} is the angular acceleration of the object at time step t_n.

IV. Implementation

To demonstrate the effectiveness of the folding palm, grasp configuration evaluation, and in-hand manipulation methods, a series of objects were selected for testing. Tasks involved grasping objects from a workbench, testing grasp stability, and manipulating objects in midair using four grasp configurations. Three objects of varying shapes and sizes were used in rotational tasks. This section highlights the reconfigurable palm features, and the experimental video includes additional shape-matching insert tasks.

A. Grasp Capacity Performance

We refer to the benchmark proposed by Jamone et al. [21] and divide the entire process into three stages: the first stage is grasping, the second stage involves throwing the object around the x-axis, and the third stage involves throwing the object around the y-axis, shown in Fig. 6. In each stage, if the object is held for at least 2 seconds without visible motion, it scores 2 points; and if the object falls or undergoes violent shaking, it scores 0 points. We conducted three repeated experiments for each grasp configuration and calculated the average score. In the evaluation of the grasping capacity, we selected the configuration with the greatest difference in palm foldability on four different objects, as shown in Table II. Notably, when grasping a bottle, a small amount of water was added to alter the center of mass during the motion, thereby better testing the grasp stability for this configuration.

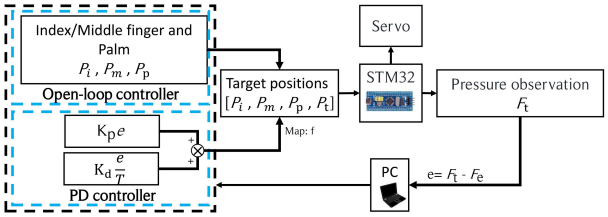

Fig. 7: Control scheme for the in-hand manipulation test.

TABLE II: Grasping Performance Scores for Objects Under Different Configurations with (F) and without (U) folding features

Object	Grasp Configuration Ω							
	(1,5)		(1,2,4)		(1,2,3,4)		(1,2,3,4,5)	
	U	F	U	F	U	F	U	F
Cube(50mm, 14g)	/	/	6	6	6	6	/	/
Apple(75mm, 24g)	0	6	6	6	6	6	6	6
Sphere(100mm,100g)	/	/	2	4	6	6	6	6
bottle(160mm, 243g)	/	/	2	4	4	6	6	6

Table II shows the grasping experiment results indicate that when the number of fingers involved in the grasp does not exceed four, palm extension effectively improves both grasp stability (with the highest scores observed in configurations with extended palms) and grasp coverage. Notably, in the configuration $\Omega = \{1, 5\}$, palm extension significantly enhances grasp stability for the apple. For cylindrical objects such as bottles, the folding palm structure allows the fingers to slightly abduct and conform to the object's surface, effectively expanding the contact area and further enhancing grasp stability. Moreover, the experiments demonstrate a positive correlation between the number of participating fingers and grasping capability. For instance, the configuration $\Omega = \{1, 2, 4\}$ successfully grasped all test objects, exhibiting improved effective grasp coverage η compared to $\Omega = \{1, 5\}$. However, for small objects such as cubes, the five-finger configuration may be less effective due to difficulties in achieving fingertip convergence. Nonetheless, once the object is securely grasped, this configuration provides the highest overall stability.

In addition to grasp stability testing, we also conducted grasping experiments on small objects (e.g., small bottles), flat objects (e.g., plates), and irregularly shaped objects (e.g., monster models and dragon fruit), demonstrating that our folding robotic hand can effectively complete grasping tasks with adaptive capabilities.

B. In-hand Manipulation Performance

As proposed in the previous Section C, to fully exploit the advantages of underactuated fingers, we apply pressure control to the thumb and position control to the index and middle fingers. During the rotation process, the forces on the index and middle fingers change passively, which significantly simplifies the force balance control for the three fingers. To enable smooth transition of the object to the fingertips, we select objects with smoothly transitioning edges.

The control framework is shown in Fig 7. The positions of the index finger, middle finger, and palm are controlled by open-loop position control, while the thumb's position is

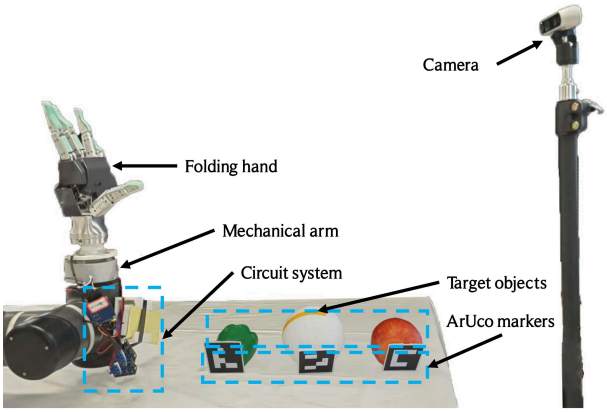

(a) In-Hand Manipulation Experimental Setup

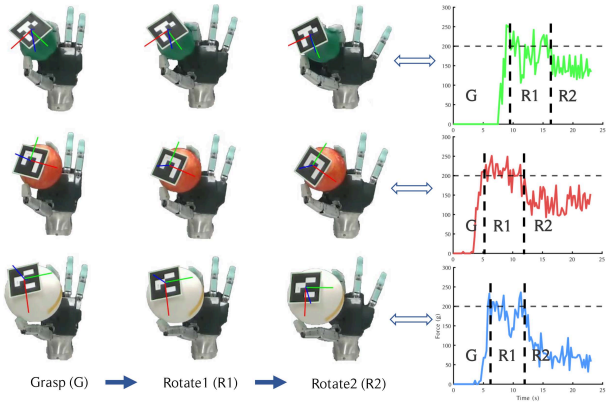

(b) The Operational Process and Variations in Thumb Force

Fig. 8: The experimental setup for in-hand manipulation and the force sensor data during the three main stages of the manipulation process.

controlled through closed-loop pressure control. The positional information of the three elements is sent from the upper computer to the lower computer to control the movement of the actuators. The lower computer returns the pressure signal, which is processed by a PD controller to generate the output signal, and, through mapping, the next position information for the thumb actuator's movement is obtained. Throughout the operation, the thumb and palm serve as active drivers, while the index and middle fingers act as passively adaptive elements. We divide the motion process into 10 discrete cycles, with the motion range extending from the fully contracted to the fully expanded state of the palm, eliminating the need for additional angle sensors and allowing for in-hand manipulation. Each object was operated three times.

The experimental setup is shown in Fig 8a, where three objects with the "smooth transition" characteristics—bell peppers, apples, and spheres—were selected. ArUco markers were attached to all objects. A Relsense D435i camera on one side was used to record the operation and detect the displacement and rotation angles of the objects. The in-hand manipulation process is shown in Fig. 8, where the object rotation is divided into three stages: the first stage, G, involves grasping the object under thumb pressure control; the second stage, R1, involves pressure control within the thumb actuator's position control range to maintain the object's stability; and the third stage, R2, is the transition phase when pressure control can no longer be maintained. It can be observed that in the R1 stage, effective pressure control is achieved, with the fingertip pressure balance set at 200g. In the R2 transition stage, the fingertip pressure initially decreases and then stabilizes, as, after the object's rotation, the thumb can no longer effectively control the pressure. However, the adaptive rotation of the thumb's base can effectively follow the object's rotation to a certain extent and maintain stable pressure, with the final actuator position ensuring the system's stability.

TABLE III: Object rotation and translation during in-hand manipulation

Object	Rotation (°)	Translation (mm)
Bell peppers(65mm, 11g)	25.1	5.66
Apple(75mm, 24g)	18.8	12.4
Sphere(100mm, 100g)	13.0	15.2

As shown in Table III, the in-hand manipulation results indicate that the control performance of the folding hand declines with increasing object volume, characterized by reduced rotation angles and increased displacement. For smaller objects such as bell peppers, the hand demonstrates excellent performance, achieving a rotation angle of 25° while maintaining displacement within 6 mm.

C. Hand Comparison

Table IV compares the developed folding hand with other existing robotic hands in terms of weight, number of actuators, anthropomorphism, reconfigurability, and in-hand manipulation capabilities.

The Shadow Hand exhibits exceptional dexterous manipulation but weighs 4200 g, resulting in high control complexity. The Barrett Hand lacks anthropomorphic design despite reconfigurable capabilities. The Hybrid Hand provides dual configurations but exhibits increased weight (1280 g) and bulky structure. The Metahand remains constrained to 3 fingers with limited anthropomorphic structure.

Our proposed folding hand uniquely combines full anthropomorphic design with efficient reconfigurability using only 6 actuators. Unlike existing designs that sacrifice anthropomorphism (Barrett Hand), require excessive actuation (Shadow Hand), or compromise weight efficiency and compactness (Hybrid Hand), our single-actuator palm folding mechanism enables coordinated finger base abduction/adduction while maintaining a complete 5-finger anthropomorphic architecture. This approach achieves superior weight efficiency (440 g) and compact design compared to other reconfigurable hands while providing spatial manipulation capabilities through biomimetic palm reconfiguration.

V. Discussion & Conclusion

The observed improvements in grasp stability and coverage of the experimental results are consistent with the evaluation of grasp capability presented in Table I. The enhanced performance in the tested grasp configurations is attributed to the folding palm structure, which alters the relative angles between fingers, thereby optimizing force distribution and increasing

TABLE IV: Comparison of representative robotic hands

Hand	Fingers	Actuators	Anthropomorphism	In-hand Manipulation	Reconfigurable	Weight
Barrett Hand [12]	3	4	Non-anthropomorphic	Yes[2]	Yes[5]	1200 g
Shadow Hand [22]	5	20	Anthropomorphic	Yes[3]	Yes[6]	4200 g
Hybrid Hand [13]	5	8	Hybrid[1]	Yes[4]	Yes[6]	1280 g
Metahand [14]	3	5	Anthropomorphic	Yes[4]	Yes[8]	Unreported
Our folding hand	5	6	Anthropomorphic	Yes[4]	Yes[9]	440 g

[1]Anthropomorphic and non-anthropomorphic. [2]Some in-hand manipulation capabilities are assumed but not specifically demonstrated. [3]Highly dexterous in-hand manipulation capabilities. [4]Planar and spatial manipulation. [5]Two finger bases rotate in-sync. [6]Opposable thumb and abduction capable MCP joints. [8]Metamorphic palm with fold/deploy configuration. [9]Single-actuator coordinated finger base abduction/adduction.

both the effectiveness and contact area of different multi-finger grasps.

In terms of in-hand manipulation, the performance degradation with increasing object volume can be explained by the mechanics of force interaction. Theoretical analysis suggests that in the R2 phase, the pressure applied to the thumb fingertip decreases as the object size increases, due to the wider angle formed between the index and middle fingers. To maintain system stability and ensure force closure, the thumb must apply less pressure. Consequently, the torque generated by the thumb is reduced, resulting in smaller final rotation angles. Although the ideal manipulation outcome would involve zero displacement of the object, maintaining precise force balance during dynamic interaction is highly challenging, making minor displacements practically unavoidable. It is worth noting that this study does not explore the scenario of in-hand manipulation involving object motion, which introduces additional analytical complexity. This will be addressed in future work.

In summary, this paper presents a compact and cost-effective anthropomorphic robotic hand that achieves palm abduction and adduction through a single actuator. The hand also enables in-hand rotational manipulation along the z-axis, allowing object reorientation without moving the robotic arm, thereby improving grasp stability and dexterity. In addition, a general grasp configuration evaluation framework is proposed for the design verification of robotic hands. Experimental results show that palm extension not only enlarges the workspace, but also increases grasp coverage. It also increases the wrapping area and improves the force distribution during grasping, thereby enhancing the grasp robustness. The compliant fingers improve the adaptability of the finger bases to object geometry. As illustrated in Fig. 1, the hand demonstrates the ability to reproduce expressive human-like gestures and perform reorientation of objects in hand during tasks such as insertion, highlighting its potential in human–robot interaction and functional manipulation. One limitation of this study is the assumption that the object's center of mass lies at the geometric center of the contact points, which may not hold true for asymmetric objects frequently encountered in real-world scenarios. Future work will explore relaxing this assumption and extending the palm mechanism to enable spatial folding, with the aim of improving motion range and manipulation functionality. The proposed design is applicable to scenarios such as healthcare, assistive devices, and human–robot interaction.

REFERENCES

[1] Y. Huang, D. Fan, H. Duan, D. Yan, W. Qi, J. Sun, Q. Liu, and P. Wang, "Human-like dexterous manipulation for anthropomorphic five-fingered hands: A review," *Biomimetic Intelligence and Robotics*, p. 100212, 2025.

[2] M. S. Han and C. K. Harnett, "Journey from human hands to robot hands: biological inspiration of anthropomorphic robotic manipulators," *Bioinspiration & Biomimetics*, vol. 19, no. 2, p. 021001, 2024.

[3] N. Zhang, P. Zhou, X. Yang, F. Shen, J. Ren, T. Hou, L. Dong, R. Bian, D. Wang, G. Gu, *et al.*, "Biomimetic rigid-soft finger design for highly dexterous and adaptive robotic hands," *Science Advances*, vol. 11, no. 17, p. eadu2018, 2025.

[4] J. Złotowski, D. Proudfoot, K. Yogeeswaran, and C. Bartneck, "Anthropomorphism: opportunities and challenges in human–robot interaction," *International journal of social robotics*, vol. 7, pp. 347–360, 2015.

[5] Y. Wang, T. Hao, Y. Liu, H. Xiao, S. Liu, and H. Zhu, "Anthropomorphic soft hand: Dexterity, sensing, and machine learning," in *Actuators*, vol. 13, no. 3. MDPI, 2024, p. 84.

[6] A. Billard and D. Kragic, "Trends and challenges in robot manipulation," *Science*, vol. 364, no. 6446, p. eaat8414, 2019.

[7] C. Gosselin, F. Pelletier, and T. Laliberte, "An anthropomorphic underactuated robotic hand with 15 dofs and a single actuator," in *2008 IEEE International Conference on Robotics and Automation*. IEEE, 2008, pp. 749–754.

[8] H. Li, C. J. Ford, C. Lu, Y. Lin, M. Bianchi, M. G. Catalano, E. Psomopoulou, and N. F. Lepora, "Tactile softhand-a: 3d-printed, tactile, highly-underactuated, anthropomorphic robot hand with an antagonistic tendon mechanism," *arXiv preprint arXiv:2406.12731*, 2024.

[9] H. Park, M. Kim, B. Lee, and D. Kim, "Design and experiment of an anthropomorphic robot hand for variable grasping stiffness," *IEEE Access*, vol. 9, pp. 99 467–99 479, 2021.

[10] D. Chu, C. Xiong, Z. Huang, J. Yang, J. Ma, J. Zhang, B.-y. Sun, and J. Cai, "Human palm performance evaluation and the palm design of humanoid robotic hands," *IEEE Robotics and Automation Letters*, vol. 9, no. 3, pp. 2463–2470, 2024.

[11] P. Capsi-Morales, G. Grioli, C. Piazza, A. Bicchi, and M. G. Catalano, "Exploring the role of palm concavity and adaptability in soft synergistic robotic hands," *IEEE Robotics and Automation Letters*, vol. 5, no. 3, pp. 4703–4710, 2020.

[12] W. Townsend, "The barretthand grasper–programmably flexible part handling and assembly," *Industrial Robot: an international journal*, vol. 27, no. 3, pp. 181–188, 2000.

[13] G. Gao, J. Chapman, S. Matsunaga, T. Mariyama, B. MacDonald, and M. Liarokapis, "A dexterous, reconfigurable, adaptive robot hand combining anthropomorphic and interdigitated configurations," in *2021 IEEE/RSJ International Conference on Intelligent Robots and Systems (IROS)*. IEEE, 2021, pp. 7209–7215.

[14] J. S. Dai, D. Wang, and L. Cui, "Orientation and workspace analysis of the multifingered metamorphic hand—metahand," *IEEE Transactions on Robotics*, vol. 25, no. 4, pp. 942–947, 2009.

[15] X. Cui, J. Sun, X. S. Zhang, S. J. Xu, and J. S. Dai, "A metamorphic hand with coplanar reconfiguration," in *2018 International Conference on Reconfigurable Mechanisms and Robots (ReMAR)*. IEEE, 2018, pp. 1–7.

[16] Q. Lu, N. Baron, A. B. Clark, and N. Rojas, "Systematic object-invariant in-hand manipulation via reconfigurable underactuation: Introducing the ruth gripper," *The International Journal of Robotics Research*, vol. 40, no. 12-14, pp. 1402–1418, 2021.

[17] Z. Li and S. S. Sastry, "Task-oriented optimal grasping by multifingered robot hands," *IEEE Journal on Robotics and Automation*, vol. 4, no. 1, pp. 32–44, 1988.

[18] L. Sievers, J. Pitz, and B. Bäuml, "Learning purely tactile in-hand manipulation with a torque-controlled hand," in *2022 International Conference on Robotics and Automation (ICRA)*. IEEE, 2022, pp. 2745–2751.

[19] T. Chen, M. Tippur, S. Wu, V. Kumar, E. Adelson, and P. Agrawal, "Visual dexterity: In-hand reorientation of novel and complex object shapes," *Science Robotics*, vol. 8, no. 84, p. eadc9244, 2023.

[20] H. Qi, A. Kumar, R. Calandra, Y. Ma, and J. Malik, "In-hand object rotation via rapid motor adaptation," in *Conference on Robot Learning*. PMLR, 2023, pp. 1722–1732.

[21] L. Jamone, A. Bernardino, and J. Santos-Victor, "Benchmarking the grasping capabilities of the icub hand with the ycb object and model set," *IEEE Robotics and Automation Letters*, vol. 1, no. 1, pp. 288–294, 2016.

[22] A. Kochan, "Shadow delivers first hand," *Industrial robot: an international journal*, vol. 32, no. 1, pp. 15–16, 2005.